Online supplementary material Appendix S1.

Åkermanite Li concentration: Details of calculations and errors

For convenience, manuscript Figure 2 is attached below.

The profile in Figure 2 was measured with the Caltech Cameca 7f instrument using conventional semiconductor-industry depth-profiling techniques (e.g., Wilson *et al.* 1989, manuscript Table 1). In order to minimise (1) effects of surface contamination and (2) distortion of the implant depth profile, the primary ($^{16}O^-$) ion beam was rastered over 100 microns. (1) SIMS primary ion current densities are inhomogeneous; consequently, without rastering, even with a field aperture and electronic gating, the tails of the beam incident on a highly contaminated surface outside of the sputter crater can contribute to the measured counting rate because the Cameca ion optics, although good, are not perfect. The efficiency of these contributions is low, but all potential contamination signal levels are frequently orders of magnitude higher than those from the implant. The rastered beam cleans the surface adjacent to the analysed area greatly reducing contamination contributions. (2) After sputtering with an unrastered beam, e.g., at the peak of the implant depth profile, the high intensity core of the beam will be deeper than the lower intensity margins. For nominal depths beyond the peak, counts will still be coming from the peak due to the tails of the beam incident on the walls of the crater, causing significant distortions of the depth profile, distortions which can be avoided by rastering the beam. Normally, raster sizes less than 75 μm are required for depth profiling in insulators to avoid excessive charging; however, a somewhat larger raster appears to have

worked in this case. Primary ion beam diameters for these analytical conditions, typically 20–30 μm, produce straight-walled, flat-bottomed sputter craters. To further enhance the quality of the depth profiles and to eliminate possible inclusion of stray counts from surface contamination or from crater walls when sputtering at the edges of the raster: (a) a 400 μm field aperture was used to reject counts from all but a 35–40 μm diameter area in the centre of the raster area, and (b) electronic gating rejected counts from the outer 30% of the rastered area. In this case the field aperture sets the size of the analysed area.

The depth scale in Figure 2 is based on measuring the sputter pit depth in åkermanite, using a stylus profilometer. To obtain an accurate pit depth measurement that corresponds to the assumed constant sputtering rate of the mineral sample we first removed the Au conducting coat that had been added to eliminate charging during the analysis. Times of analyses are corrected for the Au coat based on a well-defined breakthrough time in the ^{40}Ca profile.

The ^{6}Li counting rates in the first 20 nm are affected by surface contamination as shown by the corresponding increase in the ^{7}Li in the near surface region. However, there are also distortions from transients in RSF and in sputtering rate before steady-state sputtering is achieved. Because most of the sputtered ions are derived from the top two atomic layers (Prigge and Bauer 1980, Dumke *et al.* 1983) the transients result from the time required to change the chemical composition of the surface to a modified surface composition over a depth approximately corresponding to the implantation range of the

primary ions. In SIMS bulk analyses of homogeneous materials, these transient effects are usually mitigated by so-called pre-sputtering before quantitative analysis, but for implants, pre-sputtering is not possible because analysis should start from the sample surface in order to eliminate errors in the depth scale and loss of the implant during pre-sputtering. With implants, uncertainties from transient effects can be minimised by choosing a sufficiently high implant energy such that an insignificant fraction of the implanted ions are in the transient region. For our typical SIMS sputtering conditions, transient effects end around roughly 20 nm, so uncertainties are small with an implant that peaks at 100 nm or deeper because a very small fraction of the implant is in the transient region. In the case of Figure 2, where the implant peaks at 280 nm, uncertainties from transient effects are not significant.

The increase in the ^{6}Li profile in Figure 2 from 20 nm depth to the surface was due to surficial contamination mixed to greater depths by the action of the primary ion beam. Correction for surface contamination is negligible (< 1%) for the implant profile shown in Figure 2. If necessary, a correction for surface contamination can be made by selecting a lower limit, X_{min}, to the depth integral (manuscript Equation 3) safely beyond the contaminated portion of the profile, then adding a surface correction to the fluence set by the fractional area of the theoretical SRIM profile below X_{min}. SRIM and measured profiles do not agree perfectly, so if the necessary surface contamination fluence corrections exceed 5–8%, the SRIM profile can be modified to match the deeper parts of the measured profile. Uncertainties can be assessed by varying the parameters in the

surface correction. Also, the sample can be cleaned to reduce the surface contamination but care must be taken not to remove any of the implant.

For this analysis, ^{40}Ca was used as the matrix ion. The $^{6}Li/^{40}Ca$ at depths beyond 1400 nm reflects the intrinsic ^{6}Li of the åkermanite and represents a correction to the integral (10%) that is subtracted from the measured $^{6}Li/^{40}Ca$ profile to give the implant $^{6}Li/^{40}Ca$ profile. The uncertainty resulting from this correction was less than 1%.

By using text Equation (3), the RSF for ^{6}Li is calculated by integrating the implant $^{6}Li/^{40}Ca$ profile. On the shallow side the limits on the integral are selected to avoid surface contamination (discussed above) as well as transients. On the deep side, the limit is set by the constant $^{6}Li/^{40}Ca$ background ratio. In this case, we used 20 to 959 nm as the limits of integration. The value of the integral is insensitive to the exact choice of integration limits as long as the whole profile is measured.

Based on a measurement of a meteoritic CAI composition glass of known Li isotope composition, the RSF for ^{6}Li was corrected by 1.6% for instrumental isotope fractionation (IMF) to obtain an RSF for ^{7}Li. For elements heavier than Li, this IMF correction is smaller and can usually be neglected. The average $^{7}Li/^{40}Ca$ counting rate ratio deeper than 900 nm (well beyond the peak depth of the ^{6}Li implant) was used as the åkermanite ratio, and ^{7}Li atoms cm^{-3} calculated from the ^{7}Li RSF using Equation (2).

Using a density of 2.95 for åkermanite and $^{6}Li/^{7}Li = 0.083 \pm 0.001$ based on the deep part of the profile, a measured Li concentration in åkermanite of 0.53 ± 0.01 μg g^{-1} was obtained. The uncertainties in the calculated åkermanite Li concentration from the density and the Li isotopic abundance were less than 1%.

This example illustrates *how* an implant can be used to create a working measurement standard. As discussed in the manuscript text, the ^{6}Li implant fluence has not been independently calibrated; consequently, the 0.53 μg g^{-1} concentration, although precise, is subject to a systematic error as large as 30%; however, with appropriate calibration, the accuracy could be improved relatively easily to better than 5% (1*s*).

Based on the manuscript text and this Appendix, Table S1 is a summary of those uncertainties that arise in the analysis of an implant calibrator that differ from those when a conventional uniform RM is used. With attention to the details discussed above, the uncertainties associated with using an implant are no greater than using a conventional RM, where the main sources of error, other than potential matrix effects, are the uncertainty in the concentration of the element to be determined and variations in sensitivity not removed by matrix normalisation, e.g., differences from sample mounting or from charging.

Figure 2

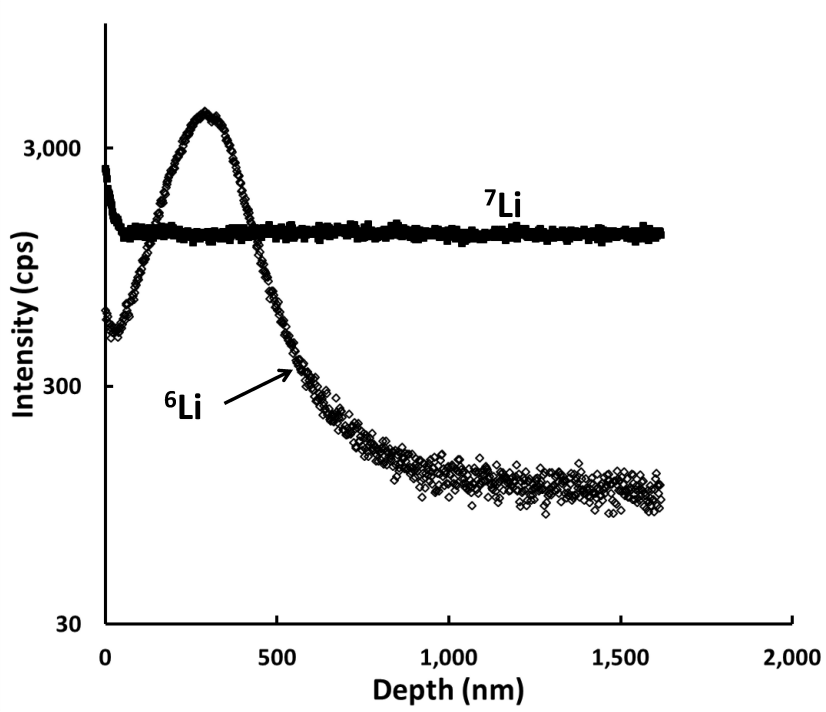
3,000
300
30
Intensity (cps)
7Li
6Li
0
500
1,000
1,500
2,000
Depth (nm)

Table S1.

Summary of sources of uncertainty

Source of uncertainty	Mitigation
Implant fluence	Minimised by calibration.
Transients at shallow depths	Implant depth ≥ 100 nm. Apply correction for lost area based on SRIM theoretical profile.
Surface contamination	Implant depth ≥ 100 nm. Implant fluence in 10^{14} cm^{-2} range. Implant minor isotope if possible. Test before implant. Apply correction for lost area based on SRIM theoretical profile. Clean sample.
Lower limit of integral	Set to eliminate errors from surface contamination or transients. Apply corrections for lost area based on SRIM profile. Test effect on integral when limit varied.
Upper limit of integral	Errors from choice small (< 1%) once full profile included. Test effect on integral when limit varied.
Background correction.	Choose peak implant concentration to be greater than 2–3 times that of background level. Errors < 1% for profiles in this paper. Test effect on integral when correction varied.
Radiation damage (Appendix S3)	Keep fluence less than 10^{15} cm^{-2}
Implant effect on RSF (Appendix S3)	Keep fluence less than 10^{15} cm^{-2}
Depth scale (profilometry)	< 2% (1*s*)
Density	< 1%
Isotopic composition of standard	< 1%
SIMS instrumental mass fractionation	< 1%

Appendix S1 References

Dumke M.F., Tombrello T.A., Weller R.A., Housley R.M. and Cirlin E.H. (1983)
Sputtering of the gallium-indium eutectic alloy in the liquid phase. **Surface Science**, **124**, 407–422.

Prigge S. and Bauer E. (1980)
Static SIMS studies of metal-covered W(110) surfaces. **Advances in Mass Spectrometry, 8**, 543–552.

Wilson R.G., Stevie F.A. and Magee C.W. (1989)
Secondary ion mass spectrometry: A practical handbook for depth profiling and bulk impurity analysis. **Wiley (New York),** 384pp.